# Fine-resolution photoacoustic imaging of the eye

Ronald H. Silverman[*a,b], Fanting Kong[c], Harriet O. Lloyd[a] ,Y. C. Chen[c]

[a]Weill Cornell Medical College, 1300 York Ave., Room LC303, New York, NY 10065
[b]Riverside Research Institute, 156 William St., New York, NY 10038
[c]Hunter College, City University of New York, 695 Park Ave., New York, NY 10065

## ABSTRACT

**Purpose**: Ultrasound and optical coherence tomography (OCT) are widely used techniques for diagnostic imaging of the eye. OCT provides excellent resolution, but limited penetration. Ultrasound provides better penetration, but an order-of-magnitude poorer resolution than OCT. Photoacoustic imaging is relatively insensitive to scattering, and so offers a potential means to image deeper than OCT. Furthermore, photoacoustic imaging detects optical absorption, a parameter that is independent of that detected by conventional ultrasound or OCT. Our aim was to develop a photoacoustic system suitable for imaging the eye.
**Methods**: We developed a prototype system utilizing a focused 20 MHz ultrasound probe with a central aperture through which optics were introduced. The prototype system produced 1-μJ, 5-nsec pulses at 532 or 1064 nm with a 20-μm spot size at a 500 Hz repetition rate. The photoacoustic probe was mounted onto computer-controlled linear stages and pulse-echo ultrasound and photoacoustic images obtained on *ex vivo* pig eyes and *in vivo* mouse eyes.
**Results**: Lateral resolution was significantly improved by use of a laser spot size much smaller than the acoustic beamwidth. Photoacoustic signals were obtained primarily from melanin in *ex vivo* tissues and from melanin and hemoglobin *in vivo*. Image fusion allowed superposition of photoacoustic signals upon the anatomic features detected by conventional ultrasound.
**Conclusion**: Photoacoustic imaging detects the presence of clinically relevant pigments, such as melanin and oxy- and deoxy-hemoglobin, and, potentially, from other pathologic pigments occurring in disease conditions (tumors, nevii, macular degeneration). Fine-resolution photoacoustic data provides information not detected in current ophthalmic imaging modalities.

**Keywords**: ultrasound, photoacoustic, eye

## 1. INTRODUCTION

The eye is unusual anatomically in providing an optical window via the cornea, pupil and lens that allows the use of optical techniques for visualizing internal structures, such as the retinal surface. The globe itself is a cyst-like structure filled with optically transparent media, the aqueous fluid (filling the anterior chamber between the lens/iris and the cornea) and the gel-like vitreous, filling the globe from the posterior lens/iris to the retina. While direct visualization of the retinal surface using tools such as indirect ophthalmoscopy is invaluable, surface imaging provides inadequate information for proper diagnosis of diseases affecting the retina, choroid and optic nerve, including age-related macular degeneration, diabetic retinopathy, glaucoma and tumors. Both ultrasound and optical technologies have been developed that provide cross-sectional images of the eye to address this requirement.

Ultrasound (US) is ideal for ocular imaging because the superficial location of the eye. The low level of acoustic attenuation produced by the aqueous and vitreous enable use of relatively high frequencies, which in turn provide fine resolution. Ophthalmic US systems typically operate with center frequencies at or near 10 MHz, allowing visualization of the globe and orbit. In the early 1990's, ultrasound biomicroscopy (UBM) utilizing frequencies in the 35–50 MHz range was introduced by Foster and Pavlin.[1] Absorption by ocular fluids and tissues is significant at

* ros2012@med.cornell.edu; phone (212)746-6106; fax (212)746-8101

Photons Plus Ultrasound: Imaging and Sensing 2010, edited by Alexander A. Oraevsky, Lihong V. Wang,
Proc. of SPIE Vol. 7564, 75640Y · © 2010 SPIE · CCC code: 1605-7422/10/$18 · doi: 10.1117/12.842471

these high frequencies, limiting UBM systems to evaluation of the anterior segment (cornea, anterior chamber, iris, ciliary body and lens). Transducers operating at 20 MHz have recently been introduced for evaluation of the retina and choroid.[2,3,4]

Optical coherence tomography (OCT) for imaging the retina was first described by Huang and his coworkers in 1991[5] and more recently extended to the anterior segment as well.[6] With resolution on the order of 10 μm, OCT systems are significantly superior to US for evaluation of the retina, which at 20 MHz provides an axial resolution of about 75 μm and lateral resolution around 200 μm. OCT, however, provides limited penetration in depth (about 1 mm), is degraded by any opacity (cataract, hemorrhage) in the eye, and can only be performed in the central fundus, i.e., that part of the retina visible through the pupil. The optical signal detected by OCT results from the presence of refractive index discontinuities, which may include connective tissues, cytoplasmic organelles, cell nuclei and melanin granules[7], structural elements that may also produce acoustic backscatter, especially at higher frequencies. UBM and OCT images thus have a generally similar appearance, since in both cases the signal results from the presence of discontinuities in tissue homogeneity.

In photoacoustic imaging (PAI)[8,9,10], a short monochromatic light pulse is directed at a tissue and absorbed by pigments at the emitted wavelength. Pressure is generated due to a deposition of energy in a tissue volume faster than it can diffuse and manifested as thermoelastic expansion occurring at the speed of sound, generating broadband US. The magnitude of the PAI signal is proportional to the local fluence and the optical absorption coefficient of the illuminated tissue at the wavelength of the light source. Images produced by this method represent optical absorption, a parameter that is independent of that imaged by US or OCT. Because optical absorption takes place with either ballistic or scattered photons, and because acoustic scattering is far weaker than optical scattering, PAI images deeper than does OCT, which is degraded by optical scattering due to its dependence on ballistic photons.

If a tissue is illuminated with an unfocused or weakly focused light source, the lateral resolution of the photoacoustic system will depend wholly on the focal properties of the US transducer used as the receiver, specifically, frequency, aperture and focal length. However, if the laser spot size is smaller than the acoustic beamwidth of the transducer, lateral resolution will be superior to that obtained with an unfocused laser to a tissue depth such that scattering causes the laser beam diameter to spread to that of the acoustic beamwidth. The mean free path of transport at 633 nm for the retina, the retinal pigment epithelium and the choroid are reported to be 1 mm, 10 μm and 86 μm, respectively.[11,12] Thus, for PAI imaging of the retina/choroid, laser focusing may prove advantageous. Focusing also allows use of a lower power laser since only a tiny spot is illuminated rather than the entire tissue. The reduced power of the laser allows higher pulse rates, since pulsed laser cycling time is largely related to cooling issues. In addition, focusing the laser prevents reception of extraneous photoacoustic signals from outside the transducer focus, which could potentially reduce signal-to-noise.

The major chromophores of the eye are melanin and hemoglobin. Melanin, present in the uvea (iris, choroid, ciliary body) and in pigmented tumors, has maximum absorption in the ultraviolet, decreasing monotonically through the visible to the near infrared (NIR).[13] Hemoglobin, present in the rich microvasculature of the optic nerve and uveal tract, in superficial microvessels of the retina and conjunctiva and in pathologic neovascularization (including tumors), has peak absorption at around 580 nm. Oxy- and deoxy-hemoglobin have distinctly different spectra, with the former peaking broadly in the NIR and the latter in the visible near 757 nm[14], and an isobestic point (where absorption coefficients are the same) near 800 nm.

PAI and US imaging can be performed simultaneously, because the US transducer can operate in either pulse-echo (PE) mode or receive only mode (for PAI). This provides a mechanism for simultaneous imaging of two independent tissue characteristics: acoustic impedance discontinuity and optical absorption.[15]

Of great interest is the potential of nanoparticles as PAI contrast agents.[16,17] Spherical gold nanoparticles of ~20-nm diameter show distinctive absorption bands in the visible due to surface plasmon oscillation of free electrons.[18] However, when gold nanoparticles are extended to a rod shape, the absorption wavelength shifts to the NIR region as laser excitation resonates longitudinally.[19,20] The intense optical absorption, minute dimension, non-toxicity, and inertness of gold nanorods (GNRs) make them an ideal means for imaging occult or transparent structures. By setting the absorption band of the GNRs to 650-900 nm in the NIR, absorption by most biologic chromophores and water can be minimized. GNRs can also be targeted to specific biomolecules, or with a polyethylene glycol (PEG) coating can be formulated to not conglomerate or attach to tissues.

PAI of the eye offers clinical significance for evaluation of retinal diseases, glaucoma and tumors. PAI will allow visualization of the spatial distribution of pigments in the retina (melanin and possibly lipofuscin and visual pigments) and especially oxy- and deoxy-hemoglobin. These may well be altered beyond normal limits in diseases such as age-related macular degeneration and diabetic retinopathy. PAI may be of particular value for characterization of small pigmented lesions, which may be benign nevii or potentially lethal melanomas. While useful, 20 MHz US provides information only on reflection and scattering in such small masses and OCT cannot penetrate. PAI, especially using NIR wavelengths, may allow a more comprehensive evaluation of such small masses, including identification of vascularity and specific absorbing molecular species such as deoxyhemoglobin associated with ischemia. Loss of vision in glaucoma is believed to result from chronic ischemic insults to the optic nerve. A capacity to visualize relative ischemia in the microvasculature of the optic nerve would be a valuable means for early diagnosis and treatment monitoring.

## 2. METHODOLOGY

We developed a prototype PAI system utilizing a focused laser to image superficial tissues. The system was composed of optical and acoustic subsystems, the photoacoustic assembly, and the scanning and data acquisition systems. The optical system utilized a passively Q-switched Cr,Nd:YAG microchip laser emitting 5-nsec pulses at 1064 nm, which was then frequency-doubled to 532 nm. A filter allows the selection of either wavelength for illumination. Pulses were emitted at a repetition rate of 500 Hz. The laser was coupled into a 25-μm core diameter fiber and focused through a micro-lens to the focal plane of a custom 20 MHz US transducer with a 12-mm aperture, 30-mm focal length and 5-mm central aperture for the optics.[21] The probe was attached to computer-controlled linear stages for scanning. The pulse energy at the sample was 1 μJ. During scanning, vectors were acquired at evenly spaced intervals of user-specified dimension. Each light pulse was detected by a photodiode and this was used for synchronization.

In PAI mode, the US pulser/receiver (Model 5900, Panametrics, Waltham, MA) was used as a passive receiver and the photodiode signal was used to trigger the digitizer. In PE mode, the laser continued to pulse as usual, and the photodiode signal was used to trigger both the US pulser and the digitizer. US data were acquired at 12-bit resolution at a sample rate of 400 MHz. Scans typically consisted of 700-800 parallel vectors spaced at 10-μm intervals.

We first scanned a 25 μm diameter aluminum wire to ascertain lateral resolution in both PE and PAI modes as a function of range. Scans were acquired at range intervals of 0.25 mm and the 6-dB width of the wire target was measured as well as the 6-dB depth of field.

We imaged fresh *ex vivo* pig eyes that were obtained from a commercial abattoir. After immersing the whole eye in normal saline solution, we imaged the anterior segment through the cornea. We next cut the eye in half with a circumferential cut along the equator. We removed the vitreous and the lens. The posterior segment was then laid face upwards, scanned and US and PAI data acquired. We then similarly scanned the region of the ciliary body by placing the anterior segment with the internal structures face-up, allowing them to be scanned photoacoustically.

Spectral parameter images of photoacoustic data were generated by determining acoustic power spectra within a 48 sample by 7 vector window that was rastered across the entire image. At each (overlapping) position, the local power spectrum was normalized against the spectrum from a bright photoacoustic source whose spectrum closely matched that of the transducer impulse response. We calculated the linear-best-fit to local normalized power spectra and determined the slope (dB/MHz) and midband-fit amplitude (dB) at the transducer center frequency (20 MHz). Spectral parameter images representing slope and midband-fit amplitude were then produced. Midband-fit images represent the signal integrated over the transducer bandwidth, and thus correspond to photoacoustic signal amplitude. Spectral slope represents frequency-dependence, which in PE acoustic backscatter is related to the scatterer diameter. Attenuation by intervening tissues, however, will decrease spectral slope because absorption increases exponentially with frequency.[22]

We conducted experiments utilizing GNRs that absorbed near 532 nm (NanoPartz, Inc. Salt Lake City UT), matching one of the two wavelengths available to us with our current instrumentation. We injected 0.25 ml of GNRs into the anterior chamber of an *ex vivo* pig eye and acquired photoacoustic data at 532 nm.

We performed photoacoustic imaging of a white mouse eye *in vivo*. This was performed by anesthetizing the mouse with intraperitoneal injection of ketamine 100 mg/kg and xylazine 10 mg/kg. A waterbath was formed within a

transparent polyethylene membrane maintained within a ringstand. After opening the mouse eye and covering it with several drops of methycellulose, the waterbath was lowered to make contact with the eye. The scanning assembly was then lowered into the waterbath and scanning performed as usual. Data were acquired from a series of parallel planes.

## 3. RESULTS

The wire target reflection at the focus measured 192 µm in PE mode. In photoacoustic mode, the width of the wire target was 24 µm at both 1064 nm and 532 nm. The photoacoustic depth-of-field was approximately 5 mm in clear media.

Fig. 1 shows photoacoustic image of the anterior segment in an intact *ex vivo* pig eye. An interesting finding is the signal produced at the surface of the lens, which, being optically transparent, would be expected to be photoacoustically invisible. We found this signal to be present at 532 nm, but absent when scanning at 1064 nm. To rule out two-photon absorption, we measured the amplitude of the photoacoustic signals from the iris and lens surfaces as a function of optical intensity. (We would expect linear and quadratic relationships between laser intensity and photoacoustic amplitude for conventional and two-photon absorption, respectively.) The results, plotted in Fig. 2, show linear relationships in both cases. Our finding suggests that since the lens is known to be quite transparent, with less than 0.003 fraction absorption through the full thickness of the lens[23], possibly a thin layer at the lens surface is absorbing strongly at 532 nm.

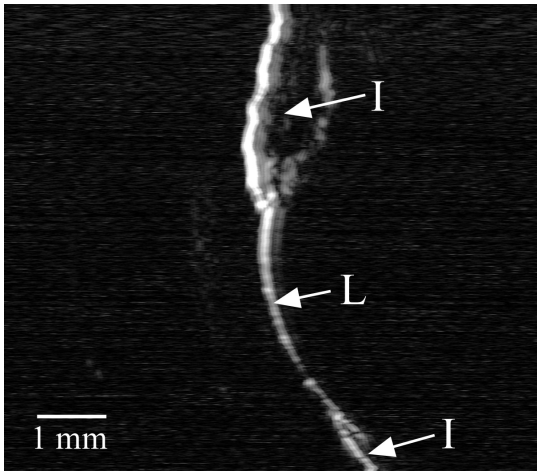


Figure 1. Photoacoustic image of anterior segment of intact *ex vivo* pig eye obtained using 532 nm pulsed laser. The depth axis is horizontal. The pigmented iris (I) generates a strong signal. The lens surface (L) is also seen within the open pupil.

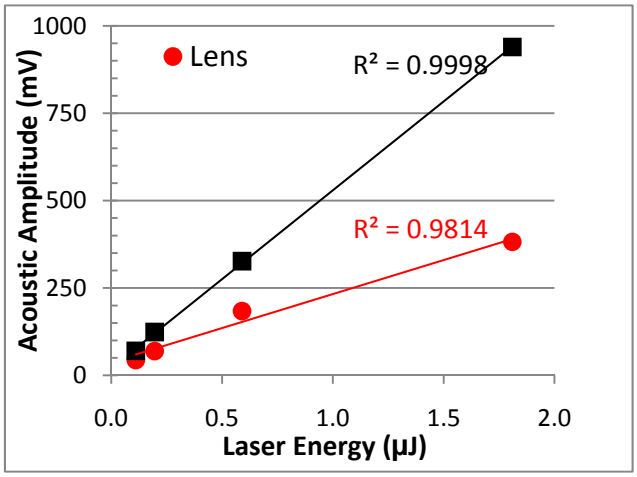


Figure 2. Plot of peak amplitude of the acoustic signal received from the surfaces of the iris and lens as a function of laser energy.

Fig. 3 compares PE-US with 532-nm photoacoustic images of the posterior of an *ex vivo* pig eye after excision of intervening anterior segment structures. In the PE image, the retina/choroid are seen as a bright surface layer. The underlying sclera appears as a solid tissue with significant speckle from acoustic phase interference. In the photoacoustic image, a single bright interface is seen which may represent the retinal pigment epithelium.

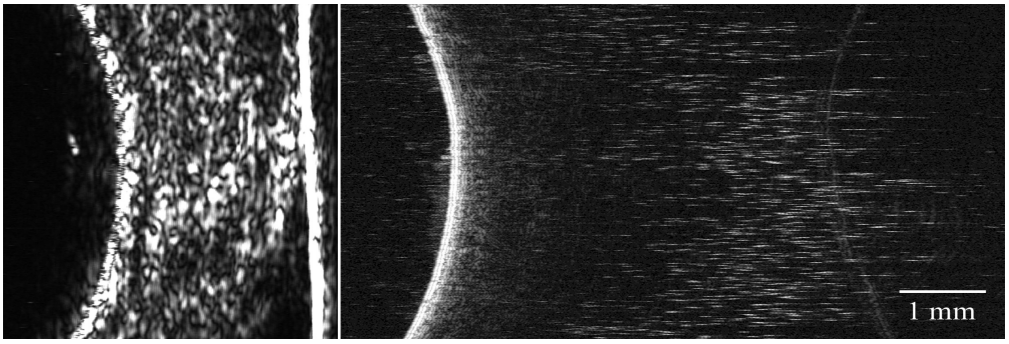


Figure 3. Pulse-echo image (left) and photoacoustic image (532 nm) of the retina/choroid of *ex vivo* pig eye after excision of the anterior segment. Note the presence of 'noise' signals appearing several millimeters behind the retina/choroid. These are most likely time-delayed signals resulting from collapse of transient photoacoustically-induced microbubbles. The flat surface appearing to the right of the pulse/echo image is the supporting pad underlying the eye.

In Fig. 4, we compare midband-fit and spectral slope images from the region of the ciliary body and iris. Seen in the image are the ciliary processes, zonular fibers and the iris pigment epithelium, which, as expected, produces a bright signal due to its high melanin content. The spectral slope image demonstrates more positive values for the deeper tissue structure, which is, in this case, the iris. Since attenuation would, if anything, cause decreased spectral slope, this observation must be attributed to some characteristic related to chromophore dimension.

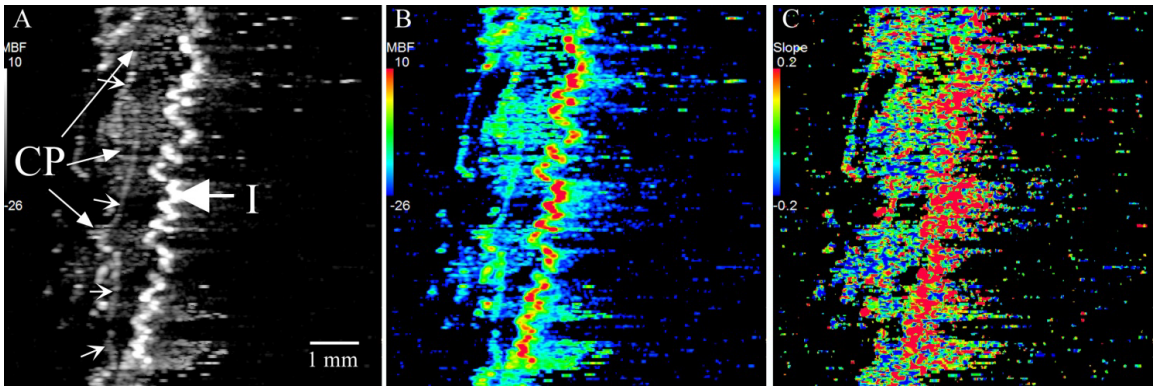


Figure 4. Spectral parameter images derived from 532-nm photoacoustic scan data of the region of the ciliary body. Depth increases from left to right. (A) and (B) are midband fit images in grayscale and color, respectively. (C) represents spectral slope, i.e., frequency dependence. In this orientation, the ciliary processes (CP), which are pigmented spoke-like structures posterior to the iris, are clearly evident. Also seen are zonular fibers (small arrows). Underlying the ciliary processes is a bright signal from the iris pigment epithelium (I), which has a corrugated or washboard surface. The spectral slope shows the iris signal to have a relatively high content of higher frequencies, as indicated by its red coloration.

A photoacoustic image of the anterior segment in an intact pig eye following injection of GNRs is shown in Fig. 5. The aqueous fluid filling the anterior chamber is normally optically and acoustically transparent. The aqueous, produced by the ciliary processes and draining through the trabecular meshwork in the iridocorneal angle, is responsible for maintenance of intraocular pressure. Increased outflow resistance results in high-intraocular pressure. GNRs may be useful as contrast agents for tracking aqueous flow dynamics in vivo, currently very difficult due to the slow flow of the transparent aqueous.

Combined pulse/echo and photoacoustic images of the living mouse eye are shown in Fig. 6. In these images, the relatively low resolution of the 20 MHz PE system provides little information beyond the presence of the globe (about 3.5 mm in axial length). Photoacoustic data were obtained on both anterior segment and orbital structures.

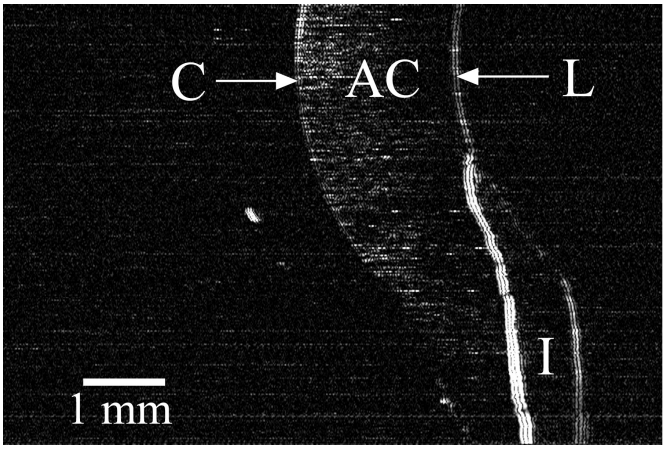


Figure 5. 532-nm photoacoustic image of anterior chamber (AC) of intact *ex vivo* pig eye after injection of gold nanorods. The nanoparticles fill the volume of the anterior chamber, outlining the surfaces of the posterior cornea (C) and the anterior lens (L) and iris (I).

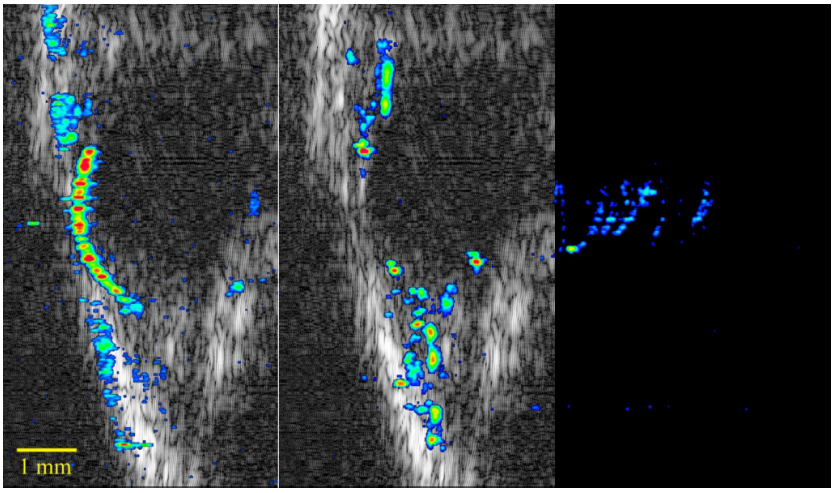


Figure 6. Images from two parallel scan planes of *in vivo* mouse eye. 20 MHz pulse/echo data are rendered in grayscale and photoacoustic data superimposed in color. In the image at left, photoacoustic signals are received from superficial tissues, possibly the periocular skin, and a bright signal is detected, possibly from iris vasculature. In the plane on the right, the iris is avoided and photoacoustic signals are detected in the orbit, probably representing vasculature.

## 4. CONCLUSIONS

We demonstrated photoacoustic imaging of the eye with a focused laser coaxial and confocal with a 20-MHz ultrasound probe. Fine-resolution images were obtained of *ex vivo* tissues in the pig eye. While melanin-containing tissues such as the retina/choroid and the iris and ciliary body produced signals as expected due to their melanin content, the anterior lens surface also produced a signal. The linear relationship between light-intensity and photoacoustic amplitude rules out non-linear processes, suggesting the presence of a thin layer containing a chromophore absorbing at 532 nm on the lens surface.

We demonstrated detection of GNRs injected into the anterior chamber. This is of interest in that such particles, at under 100 nm in length, might be used to trace aqueous outflow by measuring washout from the anterior chamber and their presence in the outflow pathway, i.e., the trabecular meshwork and Schlemm's canal. This would be especially feasible in small animal models of glaucoma, where the sclera is thin enough to allow transscleral photoacoustic imaging of these structures.

We conducted a first *in vivo* study of a mouse eye. Because of the small degree of pigmentation in the white mouse, the primary chromophore in this case was hemoglobin. Strong signals were obtained from the anterior segment and the orbit.

Clinical application of ophthalmic PAI can only be considered within the context of laser safety. For short pulsed irradiation of nanosecond duration, the dominant mechanism of laser hazard in the retina is thermal. The levels used in our system exceeded the ANSI[24] defined MPE by about a factor of 10 at 532 nm, but were comparable to MPE at 1064 nm. Near infrared wavelengths will provide better penetration than visible wavelengths such as 532 nm, and will allow greater specificity in matching specific chromophores such as oxy- and deoxy-hemoglobin. This in combination with improved detection electronics (for improved signal/noise) suggests that clinical application is feasible.

The use of a focused laser enabled us to improve lateral resolution by an order of magnitude compared to what would otherwise have been obtainable. This level of resolution is almost a requirement for clinical acceptance in ophthalmic imaging, as this is comparable to the resolution now achieved by OCT. PAI, however, provides information that is independent of that visualized with OCT or US and offers the potential for imaging the distribution of clinically significant biomolecules such as oxy- and deoxy-hemoglobin and melanin.

## ACKNOWLEDGEMENTS

Supported in part by grant UL1 RR024996 of the Clinical and Translational Science Center at Weill Cornell Medical College, the Biomedical Engineering Research Fund of the Riverside Research Institute, the Dyson Foundation and grant RR03037 from the National Center for Research Resources, a component of the NIH.

## REFERENCES

[1] Pavlin, C.J., Harasiewicz, K., Sherar, M.D. and Foster F.S., "Clinical use of ultrasound biomicroscopy," Ophthalmology 98, 287-295 (1991).

**[**2**]** Coleman, D.J., Silverman, R.H., Chabi, A., Rondeau, M.J., Shung, K.K., Cannata, J. and Lincoff, H., "High resolution ultrasonic imaging of the posterior segment," Ophthalmology 111, 1344-1351 (2004).

[3] Cannata, J., Ritter, T., Chen, W-H., Silverman, R.H. and Shung, K.K., "Design of efficient, broadband single element (20 – 80 MHz) ultrasonic transducers for medical imaging applications*,"* IEEE Trans. Ultrason., Ferroelectr., Frequ. Contr. 50(11), 1548-1557 (2003).

[4] Hewick, S.A., Fairhead, A.C., Culy, J.C. and Atta, H.R., "A comparison of 10 MHz and 20 MHz ultrasound probes in imaging the eye and orbit," Br. J. Ophthalmol. 88, 551-555 (2004).

[5] Huang, D., Swanson, E.A., Lin, C.P., Schuman, J.S., Stinson, W.G., Chang, W., Hee, M.R., Flotte, T., Gregory, K., Puliafito, C.A. and Fujimoto, J.G., "Optical Coherence Tomography," Science 254, 1178-1181 (1991).

[6] Baikoff, G., Lutun, E., Ferraz, C. and Wei, J., "Static and dynamic analysis of the anterior segment with optical coherence tomography," J. Cataract Refract. Surg. 30, 1843-1850 (2004).

[7] Tuchin, V., [Tissue optics. Light scattering methods and instruments for medical diagnosis. 2nd edition.] SPIE Press, Bellingham, WA (2007).

[8] Xu, M. and Wang, L.V., "Photoacoustic imaging in biomedicine," Rev. Sci. Instr. **77**, 041101-1-21 (2006).

[9] Kruger, R.A., "Photoacoustic ultrasound," Med. Phys. 2, 127-131 (1994).

[10] Oraevsky, A.A., Jacques, S.L., Esenaliev, R.O. and Tittel, F.K., "Laser based optoacoustic imaging in biological tissues," Proc. SPIE, 2134A, 122-128 (1994).

[11] Hammer, M., Roggan, A., Schweitzer, D. and Muller, G., "Optical properties of ocular fundus tissues – an *in vitro* study using the double-integrating-sphere technique and inverse Monte Carlo simulation," Phys. Med. Biol. 40, 963-978 (1995).

[12] Rovati, L., Cattini, S., Zambelli, N., Viola, F. and Staurenghi, G.," In-vivo diffusing-wave-spectroscopy measurements of the ocular fundus." Opt. Expr., 15, 4030-4038 (2007).

[13] Sardar, D.J., Mayo, M.L. and Glickman, R.D., "Optical characterization of melanin," J. Biomed. Opt., 6, 404-411 (2001).

[14] Wray, S., Cope, M., Delpy, D.T., Wyatt, J.S. and Reynolds, E.O.R., "Characterization of the near infrared absorption spectra of cytochrome aa3 and haemoglobin for the non-invasive monitoring of cerebral oxygenation," Biochim. Biophys. Acta, 933, 184-192 (1988).

[15] Emelianov, S.Y., Aglyamov, S.R., Shah, J., Sethuraman, S., Scott, W.G., Schmitt, R., Motamedi, M., Karpiouk, A. and Oraevsky, A.A., "Combined ultrasound, optoacoustic and elasticity imaging," Proc. SPIE, 5320, 101-112 (2004).

[16] Niidome, T., Yamagata, M., Okamoto, Y., Akiyama, Y., Takahashi, H., Kawano, T., Katayama, Y. and Niidome, Y., "PEG-modified gold nanorods with a stealth character for in vivo applications," J. Contr. Release, 114, 343-347 (2006).

[17] Pissuwan, D., Valenzuela, S.M. and Cortie, M.B., "Prospects for gold nanorods particles in diagnostic and therapeutic applications," Biotech. Gen. Eng. Rev., 25, 93-112 (2008).

[18] Schmidt, G., "Large clusters and colloid metals in the embryonic state," Chem. Rev., 92, 1709-1727 (1992).

[19] Yu, Y.Y., Chang, S.S., Lee, C.L. and Wang, C.R.C., "Gold nanorods: electrochemical synthesis and optical properties," J. Phys. Chem. B, 101, 6661-6664 (1997).

[20] Link, S., Mohamed, M.B. and El-Sayed, M.A., "Simulation of the optical absorption spectra of gold nanorods as a function of their aspect ratio and the effect of the medium dielectric constant," J. Phys. Chem. B, 103, 3073-3077 (1999).

[21] Kong, F., Chen, Y.C., Lloyd, H.O., Silverman, R.H., Kim, H., Cannata, J.M. and Shung, K.K. "High-resolution photoacoustic imaging with focused laser and ultrasonic beams," Appl. Phys. Lett., 94, 033902-1-3 (2009).

[22] Lizzi, F.L., Astor, M., Feleppa, E.J., Shao, M. and Kalisz, A. "Statistical framework for ultrasonic spectral parameter imaging," Ultra. Med. Biol., 23, 1371-1382 (1997).

[23] Lei, B. and Yao, G., "Spectral attenuation of the mouse, rat, pig and human lenses from wavelengths 360 nm to 1020 nm," Exp. Eye Res., 83:610-614 (2006).

[24] ANSI, [American national standard for safe use of lasers ANSI Z136.1-2007]. Laser Institute of America, Orlando (2007).